

**OPEN ACCESS**

## Influence of the Polymer Structure and its Crystallization on the Interface Resistance in Polymer-LATP and Polymer-LLZO Hybrid Electrolytes

To cite this article: Enrico Trevisanello *et al* 2022 *J. Electrochem. Soc.* **169** 110547

View the [article online](#) for updates and enhancements.

### ECS Toyota Young Investigator Fellowship



For young professionals and scholars pursuing research in batteries, fuel cells and hydrogen, and future sustainable technologies.

At least one \$50,000 fellowship is available annually.  
More than \$1.4 million awarded since 2015!



Application deadline: January 31, 2023

**Learn more. Apply today!**



# Influence of the Polymer Structure and its Crystallization on the Interface Resistance in Polymer-LATP and Polymer-LLZO Hybrid Electrolytes

Enrico Trevisanello,<sup>1,2</sup> Tugce Ates,<sup>3,4</sup> Stefano Passerini,<sup>3,4</sup> Felix H. Richter,<sup>1,2,z</sup> and Jürgen Janek<sup>1,2,\*</sup>

<sup>1</sup>Institute of Physical Chemistry, Justus-Liebig-University Giessen, 35392 Giessen, Germany

<sup>2</sup>Center for Materials Research (LaMa), Justus Liebig University Giessen, Heinrich-Buff-Ring 16, D-35392 Giessen, Germany

<sup>3</sup>Helmholtz Institute Ulm (HIU), Helmholtzstrasse 11, 89081 Ulm, Germany

<sup>4</sup>Karlsruhe Institute of Technology (KIT), D-76021 Karlsruhe, Germany

For many years, composite electrolytes (CEs) consisting of a mixture of inorganic solid electrolytes (ISEs) and polymer electrolytes (PEs) have been investigated as promising materials for the scalable production of solid-state batteries (SSBs). It is believed that CEs can overcome limitations of the single components, namely the low room-temperature conductivity and lithium ion transference number of PEs and the poor mechanical properties and high temperature processing necessary for ISE ceramics. To facilitate ion transport in the CE between the electrodes a low and stable charge transfer resistance between PEs and ISEs is required. In this study, we investigate by means of electrochemical impedance spectroscopy (EIS) how polymer crystallinity influences the charge-transfer resistance of hetero-ionic interfaces between polyethylene oxide (PEO)-based electrolytes and  $\text{Li}_{1.5}\text{Al}_{0.5}\text{Ti}_{1.5}(\text{PO}_4)_3$  (LATP) as well as  $\text{Li}_{6.25}\text{Al}_{0.25}\text{La}_3\text{Zr}_2\text{O}_{12}$  (LLZO) as ISEs. Crystallization of PEO based electrolytes below their melting temperature leads to an increased charge-transfer resistance. On the other hand, electrolytes based on the amorphous poly[2-(2-(2-methoxyethoxy)ethoxy)ethyl glycidyl ether] (PTG) do not show an increased charge transfer resistance. Finally, the conductivity of ISE-rich CEs is measured as a function of their temperature and composition for elucidating how the interface resistance influences charge transport in ISE-rich composite electrolytes.

© 2022 The Author(s). Published on behalf of The Electrochemical Society by IOP Publishing Limited. This is an open access article distributed under the terms of the Creative Commons Attribution 4.0 License (CC BY, <http://creativecommons.org/licenses/by/4.0/>), which permits unrestricted reuse of the work in any medium, provided the original work is properly cited. [DOI: 10.1149/1945-7111/aca125]



Manuscript received October 1, 2022. Published November 29, 2022.

Supplementary material for this article is available [online](#)

In recent years, lithium-ion batteries (LIBs) have become the market choice for portable energy storage systems thanks to their high power and energy density. Nevertheless, the demand for even better performing batteries increases as the automotive industry shifts from fossil fuels to electricity as main power source for vehicles. In the last decade, however, the physicochemical limit of this technology has almost been achieved.<sup>1</sup> This, together with the need for cheaper and more abundant raw materials, moves the focus of research towards new chemistries and electrode designs that can offer even higher performance. One of the most promising strategies is substituting the liquid electrolyte (LE) with a solid electrolyte (SE), giving rise to solid-state batteries (SSBs). These are quickly gaining interest with their promise to overcome the energy limits of LIBs by using high-capacity lithium metal anodes, while also providing better safety thanks to the non-volatile components.

The broad spectrum of SEs can be divided into two main categories: polymer electrolytes (PEs) and inorganic solid electrolytes (ISEs). Among other ISEs, the garnet  $\text{Li}_7\text{La}_3\text{Zr}_2\text{O}_{12}$  (LLZO) exhibits conductivities up to  $1 \text{ mS}\cdot\text{cm}^{-1}$  and electrochemical stability in contact with lithium metal, while the phosphate-based ISE  $\text{Li}_{(1+x)}\text{Al}_x\text{Ti}_{(2-x)}(\text{PO}_4)_3$  (LATP) has as high conductivity and is stable up to 4.4 V vs  $\text{Li}^+/\text{Li}$ , which is sufficient for contact with high-voltage cathode active materials.<sup>2–4</sup> However, both these ISEs require high temperature sintering to reach the high density needed for high  $\text{Li}^+$  conductivities and low tortuosity effects. This not only complicates cell manufacture but also limits the choice of cathode active materials (CAMs), as the high temperature drives unwanted reactions into more stable phases.<sup>5</sup> On the other hand, PEs offer simple integration into batteries as they can be easily fabricated into CAM-composites and casted as films. The main limitations of PEs are their electrochemical properties: low conductivity ( $<0.1 \text{ mS}\cdot\text{cm}^{-1}$ )

and  $\text{Li}^+$  transference number and electrochemical instability in contact with lithium metal or above 4 V, practically hindering their implementation at room temperature.

The combination of PEs and ISEs has received interest from the research community as layered cell design or composites might overcome the respective individual limitations.<sup>6</sup> Several publications report enhanced properties such as conductivity or redox stability of the composites over the pristine PEs,<sup>7</sup> but detailed studies and in-depth explanations of the mechanisms leading to improved transport or stability are yet relatively scarce.<sup>8–11</sup> Furthermore, the influence of polymer crystallinity on the charge-transfer resistance is rarely explored, with comparisons available only between liquid electrolytes and solid polymer electrolytes.<sup>12–14</sup> While Kalnaus et al. showed that an amorphous, more conductive, PE layer at the interface with the ISE could explain the improved performance, comprehensive electrochemical modelling that accounts for better understanding of ion movement across phase boundaries is missing.<sup>15</sup> As good contact between the two electrolytes and fast  $\text{Li}^+$  transfer across the interface is necessary for achieving satisfactory performance, we consider this as serious gap of knowledge.<sup>6,8</sup>

Several methods can be used to determine the charge transfer (CT) resistance between PEs and ISEs. The most straightforward one consists in the assembly of dense layers of the two electrolytes stacked together in 2D geometry, allowing for precise control over the geometrical contact area. Electrochemical impedance spectroscopy (EIS) then allows the assignment of different characteristic features in the acquired spectra to specific electrochemical processes taking place in the device. However, the choice of the electrode plays a big role on which lithium transport processes can be observed by EIS. With blocking electrodes, the low frequency polarization at the metal surface often superimposes with the interfacial process, as both share similar capacitances in the  $\mu\text{F}/\text{cm}^2$  range. This issue is mostly avoided by employing reversible electrodes, but the charge transfer at the electrodes might overlap with the charge transfer between the two electrolytes even in this

\*Electrochemical Society Member.

<sup>z</sup>E-mail: [Felix.H.Richter@pc.jlug.de](mailto:Felix.H.Richter@pc.jlug.de); [Juergen.Janek@pc.jlug.de](mailto:Juergen.Janek@pc.jlug.de)

case. Therefore, reference electrodes (RE) need to be added to separate the electrode contribution from the PE|ISE interfacial contribution by effectively probing the electrochemical potential away from the polarization source.

In the literature, the interface resistance between the extensively studied polymer electrolyte based on polyethylene oxide (PEO) and lithium bis(trifluoromethanesulfonyl)imide (LiTFSI) and several ISEs has been reported. For the oxide-type ISE, LLZO, the normalized values range from  $180 \Omega\cdot\text{cm}^2$  (EO:LiTFSI = 15) to  $900 \text{ k}\Omega\cdot\text{cm}^2$  (EO:LiClO<sub>4</sub> = 20) at 30 °C, depending on the salt concentration or treatment of the ISE surface.<sup>16–18</sup> All of these measurements were carried out with blocking electrodes. In the case of the phosphate-type ISE, LAMP, data are available for the lithium-ion conducting glass-ceramic produced by Ohara Corporation. The interface resistance determined by Chen et al. is  $R_p = 42 \Omega\cdot\text{cm}^2$  (EO: LiCF<sub>3</sub>SO<sub>3</sub> = 16) at 70 °C;<sup>14</sup> Zhang et al. found a value of  $R_p = 200 \Omega\cdot\text{cm}^2$  (EO: LiTFSI = 18) at 60 °C while recently James Alfred, et al. determined the charge transfer resistance to be  $R_p = 38 \Omega\cdot\text{cm}^2$  (EO: LiTFSI = 12) at 70 °C.<sup>19,20</sup> The significant scatter of the reported values demonstrates the experimental difficulties encountered while determining the PE|ISE interface resistance, with the discrepancies not only attributable to the different conducting salts employed. Interestingly, similar issues were encountered while investigating the interface between liquid electrolyte (LE) and ISE, and were only overcome by the development of four-electrode setups.<sup>13,21,22</sup> Recently, Simon et al. developed a four-electrode setup that could successfully separate the PE|Li electrode contribution from the PEO|Li<sub>6</sub>PS<sub>5</sub>Cl interface contribution in a polymer cell.<sup>9,23</sup>

In this work, we investigate the electrochemical properties of the interface between polyether-based PEs and the inorganic solid electrolytes LLZO and LAMP. The separation of different PE|ISE processes is possible through the combination of EIS and a four-electrode setup.<sup>9</sup> The influence of polymer crystallization on the ion dynamics at the interface is explored by comparing electrolytes based on PEO and amorphous poly[2-(2-(2-methoxyethoxy)ethoxy)ethyl glycidyl ether] (PTG). Contrary to the linear PEO, the four ethylene oxide units in PTG side chains prevent its crystallization.<sup>24,25</sup> Finally, the conductivity of ISE-rich CEs is measured as a function of temperature and composition, elucidating how the interface resistance between polymer and ISE influences charge transport in composite electrolytes.

## Experimental

**Materials.**—Nitric Acid (65%, Merck), titanium (IV) isopropoxide (97%, Sigma-Aldrich), citric acid monohydrate ( $\geq 99.0\%$ , Sigma-Aldrich), LiNO<sub>3</sub> (99.99% Sigma-Aldrich), aluminium nitrate nonahydrate (99.997%, Sigma-Aldrich), ammonium dihydrogen phosphate ( $\geq 99.99\%$ , Sigma-Aldrich), Li<sub>2</sub>CO<sub>3</sub> ( $>99.0\%$ , Sigma-Aldrich), ZrO<sub>2</sub> nanopowder ( $<100 \text{ nm}$ , Sigma-Aldrich), La(OH)<sub>3</sub> (99.9%, Sigma-Aldrich), Al<sub>2</sub>O<sub>3</sub> (99.8%, abcr), ( $\pm$ )-epichlorohydrin (99%, Sigma-Aldrich), tetrabutylammonium hydrogen sulphate (97%, Alfa Aesar), triethylene glycol monomethyl ether ( $>97\%$ , Sigma-Aldrich), 2-methyl-2-butanol ( $>99\%$  anhydrous, Sigma-Aldrich), P<sub>4</sub>-*t*-Bu ( $\sim 0.8 \text{ M}$  in hexane, Sigma-Aldrich), polyethylene oxide ( $M_w = 4 \times 10^6 \text{ g}\cdot\text{mol}^{-1}$ , Dow Chemical), LiTFSI ( $>99\%$  battery grade, 3 M), lithium foil (60  $\mu\text{m}$ , Honjo Japan).

**Synthesis of Li<sub>1.5</sub>Al<sub>0.5</sub>Ti<sub>1.5</sub>(PO<sub>4</sub>)<sub>3</sub>.**—Li<sub>1.5</sub>Al<sub>0.5</sub>Ti<sub>1.5</sub>(PO<sub>4</sub>)<sub>3</sub> was synthesized with a sol-gel procedure similar to the one Ma et al. reported previously.<sup>26</sup> Initially, 17 g of titanium (IV) isopropoxide were added under stirring to 100 ml of deionized water. The white TiO<sub>2</sub>/Ti(OH)<sub>2</sub> precipitate was filtered, washed with deionized water and dissolved in 150 ml of 2 M freshly prepared nitric acid. Successively, 25 g of citric acid monohydrate, 4.137 g of LiNO<sub>3</sub>, 7.506 g of Al(NO<sub>3</sub>)<sub>3</sub>·9 H<sub>2</sub>O were added to the solution. Gelation occurred after the final addition of 13.804 g of NH<sub>4</sub>H<sub>2</sub>PO<sub>4</sub>. The gel

was dried for 48 h at 90 °C, crushed and calcined in air heating at  $2 \text{ }^\circ\text{C}\cdot\text{min}^{-1}$  to 650 °C for 3 h to give white powders.

To reduce particle agglomeration, the calcined powder was ball-milled using 3 mm ZrO<sub>2</sub> milling media at 120 rpm for 6 h with mass ratios of LAMP:EtOH:ZrO<sub>2</sub> equal to 1:1.5:20. After ethanol evaporation, 250 mg of powders in a 13 mm cylindrical mold were uniaxially shaped at 150 MPa and then isostatically pressed at 500 MPa for 30 min. The obtained pellets were sintered by heating at  $2 \text{ }^\circ\text{C}\cdot\text{min}^{-1}$  to 950 °C for 5 h in air, achieving samples with  $>97\%$  of the (geometrical) theoretical density ( $\varnothing \approx 11 \text{ mm}$ , thickness  $\approx 1 \text{ mm}$ ). Each surface of the pellets was polished with SiC paper up to P4000, ultrasonicated for 10 min in acetone and recrystallized by heating at  $2 \text{ }^\circ\text{C}\cdot\text{min}^{-1}$  to 900 °C without holding the temperature. SEM images of the surface of polished and annealed pellets are shown in Fig. S1.

The LAMP powders used in the composite were prepared by heating the milled powders in an alumina crucible to 900 °C with a heating ramp of  $2 \text{ }^\circ\text{C}\cdot\text{min}^{-1}$  in air. To again reduce particle agglomeration, the obtained powders were hand ground for 15 min in an agate mortar before being vacuum dried overnight (120 °C) and transferred inside an Ar filled glovebox.

**Synthesis of Li<sub>6.25</sub>Al<sub>0.25</sub>La<sub>3</sub>Zr<sub>2</sub>O<sub>12</sub>.**—Li<sub>6.25</sub>Al<sub>0.25</sub>La<sub>3</sub>Zr<sub>2</sub>O<sub>12</sub> powders were prepared through a solid-state reaction. Stoichiometric amounts of Li<sub>2</sub>CO<sub>3</sub>, La(OH)<sub>3</sub>, Al<sub>2</sub>O<sub>3</sub> and ZrO<sub>2</sub> were hand mixed in a mortar and then ball-milled at 350 rpm, with 3 mm ZrO<sub>2</sub> and a LLZO:ZrO<sub>2</sub> ratio of 1:10, for 24 cycles with intermediate cooling times (every 10 min for 20 min). The homogenized powder was then pressed into pellets and calcined inside a tube furnace at 1000 °C for 4 h under a 150 sccm flow of dry oxygen. Calcined pellets were ground to powder and ball-milled with the previous parameters, but for a total of 40 cycles. Then, 600 mg of the obtained powder was isostatically pressed into 10 mm pellets at 400 MPa for 1 h. The resulting pellets were placed inside a MgO crucible, covered with excess powder and sintered (5 h at 900 °C, 5 h at 1100 °C and 15 h at 1230 °C, with rates of  $100 \text{ }^\circ\text{C}\cdot\text{h}^{-1}$ ) in a tube furnace under 150 sccm of dry oxygen. The resulting pellets had a diameter of approximately 8 mm, with  $95 \pm 1\%$  relative density ( $\varnothing \approx 9 \text{ mm}$ , thickness  $\approx 3 \text{ mm}$ ).

**Synthesis of 2-(2-(2-methoxyethoxy)ethoxy)ethyl glycidyl ether (triethylene glycol glycidyl ether, TG).**—The monomer TG was synthesized as described by Kim et al. through a Williamson reaction.<sup>27</sup> Briefly, 74 g of epichlorohydrin, 5.0 g of [CH<sub>3</sub>(CH<sub>2</sub>)<sub>3</sub>]<sub>4</sub>NHSO<sub>4</sub> tetrabutylammonium hydrogen sulphate and a 50 wt% sodium hydroxides water solution were mixed and cooled with an ice bath. Afterwards, 36 g of CH<sub>3</sub>(OCH<sub>2</sub>CH<sub>2</sub>)<sub>3</sub>OH was added over the course of 1 h and the emulsion was allowed to reach room temperature and stirred for 16 h. The products were extracted with ethyl acetate, dried with sodium sulphate, filtered and then solvents were removed under vacuum. The crude TG was distilled twice (b.p. 120 °C,  $\sim 0.1 \text{ mbar}$ ) under CaH<sub>2</sub> and stored under argon with 3 Å molecular sieves. TG: <sup>1</sup>H-NMR (400 MHz, CDCl<sub>3</sub>):  $\delta$  (ppm) 2.58 (m, 1H), 2.77 (t, 1H, J = 9.2), 3.1–3.18 (m, 1H), 3.35 (s, 3H), 3.37–3.79 (m, 14H).

**Synthesis of poly[2-(2-(2-methoxyethoxy)ethoxy)ethyl glycidyl ether] (PTG).**—Polymerization of TG was carried out under argon, all reagents were pre-dried with 3 Å molecular sieves in an argon filled glovebox. Firstly, 20 ml of toluene, 100  $\mu\text{l}$  of 2-methyl-2-butanol and 1.2 ml of P<sub>4</sub>-*t*-Bu solution were consecutively added to a Schlenk round-bottom flask. Afterwards, 25 g of TG was added and the solution was stirred in a water bath at 20 °C for 16 h. The polymerization was stopped by addition of 1 ml of benzoic acid in toluene, diluted in dichloromethane and passed through basic alumina to separate benzoic acid and leftovers of P<sub>4</sub>-*t*-Bu. Solvents were removed with a rotary evaporator and the residue was vacuum dried in a Buchi oven at 120 °C overnight. The obtained PTG was stored with 3 Å molecular sieves in argon. PTG: <sup>1</sup>H-NMR (400 MHz, CDCl<sub>3</sub>): 3.35 (s, 3H), 3.37–3.79 (m, 16H).

**Polymer electrolytes preparation.**—PEO was vacuum dried for 48 h at 50 °C in a vacuum oven (Büchi mod. B-585 Drying). LiTFSI was dried for 24 h at 120 °C under high vacuum ( $10^{-7}$  bar). All materials were handled in a dry room (dewpoint < -70 °C) and stored under vacuum atmosphere to prevent aging effects. The polymer electrolyte was prepared in 2.000 g batches containing 1.394 g PEO and 0.606 g LiTFSI, corresponding to a 1:15 ratio of Li:EO. The powders were mixed giving a paste-like material which was then annealed at 100 °C (overnight) and, successively, hot-pressed (Servitec Polystat 200 T press) at 100 °C and 50 kN ( $50\text{--}750\text{ kg}\cdot\text{cm}^{-2}$ ) to obtain PE films with a thickness of around 100  $\mu\text{m}$ .

In the preparation of the electrolytes based on PTG, five ethylene oxide (EO) units per monomer were accounted for, equal to the number of oxygen atoms in each monomer. In an argon filled glovebox, calculated quantities of PTG and LiTFSI were mixed according to the predefined EO:Li ratio in a vial. The solution was stirred overnight until complete dissolution of the salt.

**PTG-LATP composite electrolytes preparation.**—Inside and Ar filed glovebox, small amounts of PTG-based electrolyte (20 mg–100 mg) were directly added to an agate mortar on a weighting scale. Afterwards, LATP powders were added to bring the total weight to 1 g and the mixture was gently ground for 10 min, resulting in a dense paste.

**Characterization methods.**—*Scanning electron microscopy (SEM).*—Images were recorded with a ZEISS Merlin field-emission SEM. The samples were prepared in an argon-filled glovebox by fixing the powders or pellets on adhesive carbon tape. A secondary electron detector was used for imaging, at an extraction current and voltage of 5 kV and 1 nA.

*X-ray powder diffraction (XRD).*—A Panalytical Empyrean diffractometer equipped with a Cu  $K_{\alpha}$  X-ray tube was used to confirm the crystal structure and phase purity of the synthesized materials. In Bragg-Brentano geometry, the diffractograms were collected in the  $2\theta$  range between 10° and 90°, with a resolution of 0.026° and an integration time of 300 s/point. Soller slits and divergence slits of 0.02 rad and 1°, respectively, were employed.

*ATR-FTIR.*—The data were measured on a Thermo Scientific Nicolet iS5, equipped with the iD5 diamond crystal attachment in attenuated total reflectance (ATR) geometry. The spectra were recorded at resolution of  $4\text{ cm}^{-1}$  in the wavenumber range between  $400\text{ cm}^{-1}$  to  $4000\text{ cm}^{-1}$ .

**Cell assembly and EIS characterization.**—The ionic conductivities of the single electrolytes were determined by EIS with symmetrical blocking electrodes for the solid electrolytes, whereas a closed-cup cell with calibrated cell-constant (TSC 1600, rhd instruments) was used for the PTG electrolytes. Gold was evaporated on both surfaces of the CEs, while for the SPEs nickel disks ( $\varnothing = 9\text{ mm}$ ) were used as electrodes. To investigate a single interface, symmetrical cells Li|PE|CE|PE|Li with reference electrodes (RE) between the PE layers were prepared. The same configuration was used for PTG electrolytes, where 20  $\mu\text{l}$  of solution was infiltrated on a glass fiber separator.

The conductivity of the composite electrolyte was measured by EIS in a previously described in-house designed cell.<sup>28</sup> For each measurement, 100 mg of composite was sealed in the cell between polished stainless steel electrodes and densified for 1 min at 30 kN (380 MPa).

The reference electrodes consisted of a gold-plated tungsten wire ( $\varnothing = 25\ \mu\text{m}$ ), as after applying a cathodic current (lithium reduction) either the Li-Au alloys or plated lithium metal offer a stable potential.<sup>23</sup> The polymer layers embedding the REs ( $\varnothing = 10\text{ mm}$ ) were attached on both sides of the CE pellet ( $\varnothing = 11\text{ mm}$  approx.), followed by lithium foil ( $\varnothing = 8\text{ mm}$ ) and nickel current collectors.

The assembled cells were placed and sealed in an aluminum-laminated pouch bag. In order to have a reference electrode with a stable potential, lithium was alloyed and then plated on the gold-coated wires by applying a negative current ( $\sim 1\text{ mA cm}^{-2}$ ) between wire and lithium metal electrodes. For PEO-based electrolytes, RE preparation and cell validation were performed at 60 °C in a temperature-controlled climate chamber. A typical potential contour is shown in Fig. S2.

The high room temperature conductivity of PTG based electrolytes allowed pre-lithiation of the RE: the wire was placed between two PTG-filled glass fiber separators and the lithium metal anode and pre-lithiated in the glovebox. Afterwards, two Li|PTG|ref.|PTG units were stacked on both sides of the CE to obtain the Li|PE|CE|PE|Li cell configuration. Cells containing PTG were then quickly sealed, moved out of the argon-filled glovebox and placed in a controlled environment climate chamber at 0 °C for further measurements. Temperature-dependent impedance spectra were recorded to determine activation energies by increasing the temperature by 5 K with each step and 1 hour of equilibration time. The impedance data were fitted with the software RelaxIS (rhd instruments, Germany). Potentiostatic spectra were measured between 100 kHz and 0.1 Hz, with a perturbation potential of 10 mV recording 10 points per decade using a VMP3 or VMP300 (BioLogic, France).

## Results

**Characterization of the electrolytes.**—To investigate the influence of the chemical structure and morphology of the polymer electrolyte on the interface resistance with ISEs, two different polymers were employed. As counterpart to the typical PEO, the synthesized PTG is characterized by side chains with four ethylene oxide units, preventing its crystallization (Figs. 1a–1b).<sup>27</sup> The structures and purity of the monomer TG and polymer PTG were verified by NMR (Fig. S3). To prevent inconsistencies in the normalized values of interface resistance due to polymer electrolyte infiltration, dense pellets of LATP and LLZO were used with geometrical densities determined to be 97% and 95%, respectively. These pellets were employed as model system to investigate lithium transport across the ISE|PE interface. The phase purity of LATP and LLZO was confirmed by XRD data, as well as the crystallinity of a PEO based electrolyte and amorphous nature of the PTG based one (Fig. S4).

The conductivity data of the individual electrolytes at different temperatures are presented in Fig. 1. The PEO-based electrolyte shows a strong reduction in conductivity below its melting point, while the PTG-based electrolyte is characterized by a much smoother decrease. The total ionic conductivities of the ISEs, the sum of the bulk and grain boundary contributions, are at least one order of magnitude higher than those of the polymers. The conductivity of the PEO-based polymer electrolyte also agrees with previous reports, showing a steep decrease in the electrical properties below its melting temperature of about 45 °C. This was associated with the crystallization of PEO or  $\text{EO}_6\text{:Li}_1$  units.<sup>29</sup> The measured activation barriers for LATP, LLZO and PEO (above 45 °C) based on the total conductivity are  $E_a = 0.33\text{ eV}$ ,  $0.34\text{ eV}$  and  $0.42\text{ eV}$ , respectively. To the best of our knowledge, the conductivity of linear PTG was not yet studied as a function of both the concentration of LiTFSI and temperature. The data in Fig. S5 show the known trend for glass-forming electrolytes, where the increased viscosity and  $T_g$  at high concentration of salt leads to a decrease of the total conductivity.<sup>30</sup> All of these values are in good agreement with those previously reported, with LATP and LLZO having total conductivities one order of magnitude higher than the PEs over the whole range of temperatures investigated.

**Electrochemical characterization of the PEO-ISE interfaces.**—To characterize the interfaces, we employed the same cell configuration used by Simon et al. for the investigation of the interface

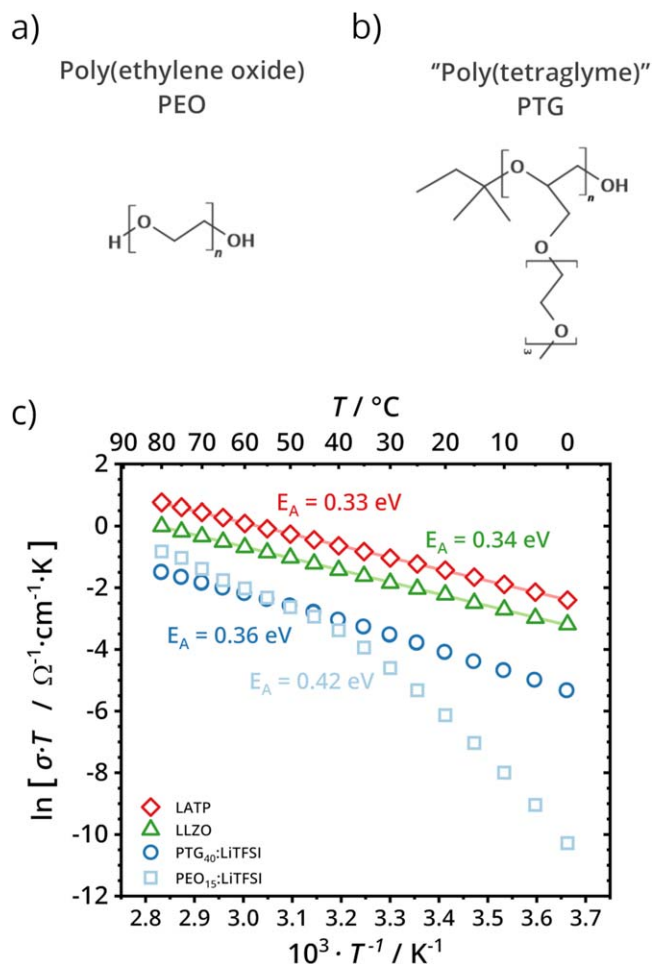


**Figure 1.** Chemical structure of the polymers used in this study: (a) poly (ethylene oxide) (PEO) and (b) poly(2-(2-(2-methoxyethoxy)ethoxy)ethyl glycidyl ether), shortened to poly(tetraglyme) (PTG) for its close resemblance to the oligo-ether solvent. (c) Arrhenius plot for the electrolytes used in this work: L ATP, LLZO, PTG<sub>40</sub>:LiTFSI, and PEO<sub>15</sub>:LiTFSI.

between a PEO based electrolyte and Li<sub>6</sub>PS<sub>5</sub>Cl solid electrolyte.<sup>9</sup> A detailed description of the measurement setup and data recorded are reported in Fig. S6. The properties of the electrochemical contact between the ISEs and the PEO-based PEs were measured with the four-electrode method. Nyquist plots of the EIS data recorded at 60 °C for the Li|PEO, PEO|L ATP and PEO|LLZO interfaces are shown in Figs 2a, 2c, 2e, respectively. The data were normalized to the (geometric) contact area between ISE and PE, with both sides of the pellet accounted for by dividing the obtained resistance value by two (series connection). Equivalent circuit models of the electrochemical system are illustrated on the bottom right of each plot, with the necessary introduction of constant phase elements to account for geometric and chemical inhomogeneity on the surface.<sup>31</sup>

The nature of the electrochemical process can be assigned by combining information about the normalized capacitance and relaxation time. The relatively fast bulk transport of ions is usually observed at high frequencies of the spectrum where the “bulk” resistances of the electrolytes are evaluated. This value in the sandwiched setup corresponds well to the sum of the bulk resistances of all electrolytes, measured separately beforehand. The mid-frequency regions of the Nyquist plots each show one semicircle. The capacitances and characteristic frequencies for the corresponding processes are 2.7  $\mu\text{F}\cdot\text{cm}^{-2}$  and 1.1 kHz for the cell with L ATP, as well as 0.43  $\mu\text{F}\cdot\text{cm}^{-2}$  and 0.8 kHz for the cell containing LLZO. These values match with the results of Zhang et al. for L ATP, and Langer et al. for LLZO, and they were attributed to the

lithium ion transfer at the interface.<sup>17,19</sup> Also the Li|PEO interface shows similar values, with a specific capacitance and characteristic frequency of 1.3  $\mu\text{F}\cdot\text{cm}^{-2}$  and 1.1 kHz. The characteristic frequencies of these processes are all very similar and can be attributed to the Li|PE and PE|ISE electrolyte interfaces. It has to be noted that on the surface of Li metal decomposition products of the PE likely formed a solid electrolyte interphase (SEI), explaining the similar values of capacitance and characteristic frequencies observed PE|ISE contacts. Overall, the obtained values are in good agreement with those reported previously.<sup>12,18,21</sup> In the low frequency region, a depressed semicircle was measured at the LLZO|PEO interface, while a line close to 45° of inclination was observed for the L ATP|PEO interface. The difference of the two contacts is likely due to the formation of an interphase between LLZO and the polymer electrolyte as discussed later.

The charge transport across all interfaces studied here are characterized by quite close activation energies:  $E_a = 0.76 \text{ eV}$ , 0.72 eV and 0.67 eV for Li|PEO, LLZO|PEO and L ATP|PEO, respectively (Fig. 3a). The quite similar values of activation energy and normalized resistance for the Li|PEO interface compared to the two other ISEs suggest similar lithium-ion dynamics at the SEI formed on top of the lithium metal. Interestingly, a deviation from linearity below 45 °C was observed for all samples. At this temperature, the concurrent steep increase of the “bulk” resistance (Fig. S7) suggests that crystallization of the polymer electrolyte causes its deviation towards lower values. This is widely reported in the literature and matches with the conductivity trends seen in the previous section (Fig. 1).

However, the deviation from linearity of the interfacial region is less pronounced compared to the bulk. At the PE|ISE interface, the reorganization of polymer chains is likely hindered by reduced free volume close to the surface of the ISE, leading to a slower nucleation/growth of the crystalline phase.<sup>32</sup> Another effect that can lead to hindered crystallization is the higher concentration of ions at the interface linked to the double layer present at the PE|ISE interface. Both effects can hinder the crystallization process, keeping a significant fraction of the polymer in an amorphous, more conductive state. To exclude the influence of polymer crystallization on the ion transport at the interface, the electrochemical properties of the interface with a PTG-based electrolyte are investigated in the next section.

#### Electrochemical characterization of the PTG-ISE interfaces.—

The interface resistance for the lithium-ion transfer between PTG and the ISEs was studied with the same four-electrode setup (Fig. S6). As previously described, the side chains in PTG prevent its crystallization below 45 °C. Therefore, it is well suited to study the interfacial dynamics of ether-based polymers. Furthermore, thanks to the high room-temperature conductivity of the PTG electrolyte, it was possible to prepare the RE before bringing the polymer electrolyte and the ISEs in contact with each other. This allowed us to measure the cell characteristics within few minutes from their first coming in contact.

Nyquist plots recorded at 60 °C for the Li|PTG, PTG|L ATP, and PTG|LLZO interfaces are shown in Figs. 2b–2d–2f, respectively. As previously described, the high frequency region corresponds to the fast transport in the bulk of the electrolytes (Fig. S8). The process observed in the mid-frequency region can be assigned to the charge transfer at the interface. The characteristic capacitances for these processes are 2.0  $\mu\text{F}\cdot\text{cm}^{-2}$  for the cell with L ATP, 1.8  $\mu\text{F}\cdot\text{cm}^{-2}$  for the cell containing LLZO and 0.44  $\mu\text{F}\cdot\text{cm}^{-2}$  for the lithium electrode. As expected, the capacitance values match well with the ones previously determined for the PEO based electrolytes, but also the ones determined for liquid electrolytes.<sup>13,22</sup> PEO and PTG have similar conductivities and coordination spheres for the Li<sup>+</sup> at this temperature, leading to similar double-layer capacitance in proximity of the ISE and SEI on the lithium anode. However, the resistance and consequently the characteristic frequency of the interfacial processes are different from the ones found at the PEO interface. The determined

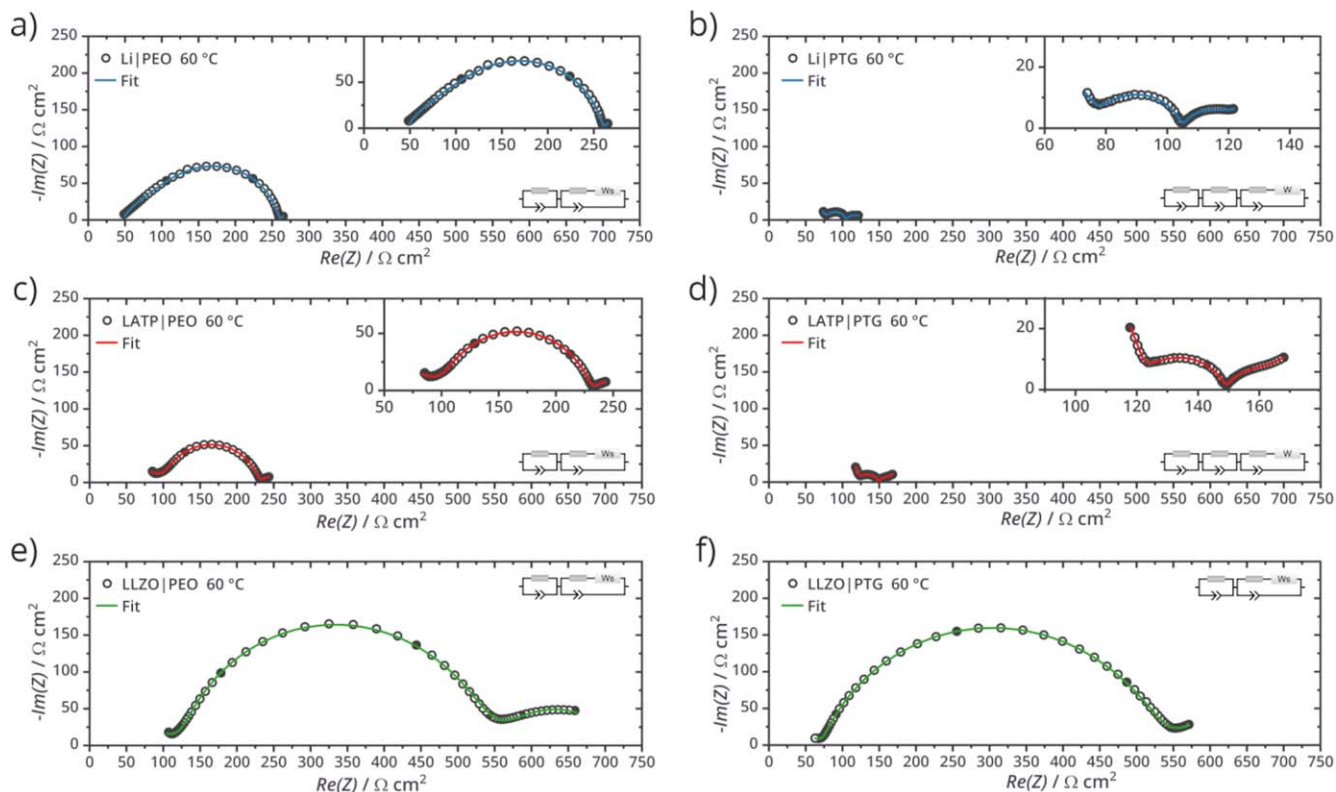


**Figure 2.** Electrochemical characterization of the polymer-ISE interfaces. Nyquist plots with the area normalized impedance data for the (a) Li|PEO, (b) Li|PTG, (c) PEO|LATP, (d) PTG|LATP, (e) PEO|LLZO, and (f) PTG|LLZO interfaces at 60 °C. The inset plots show a magnification of the data. Equivalent circuits used to model the spectra are reported on the top right of each plot.

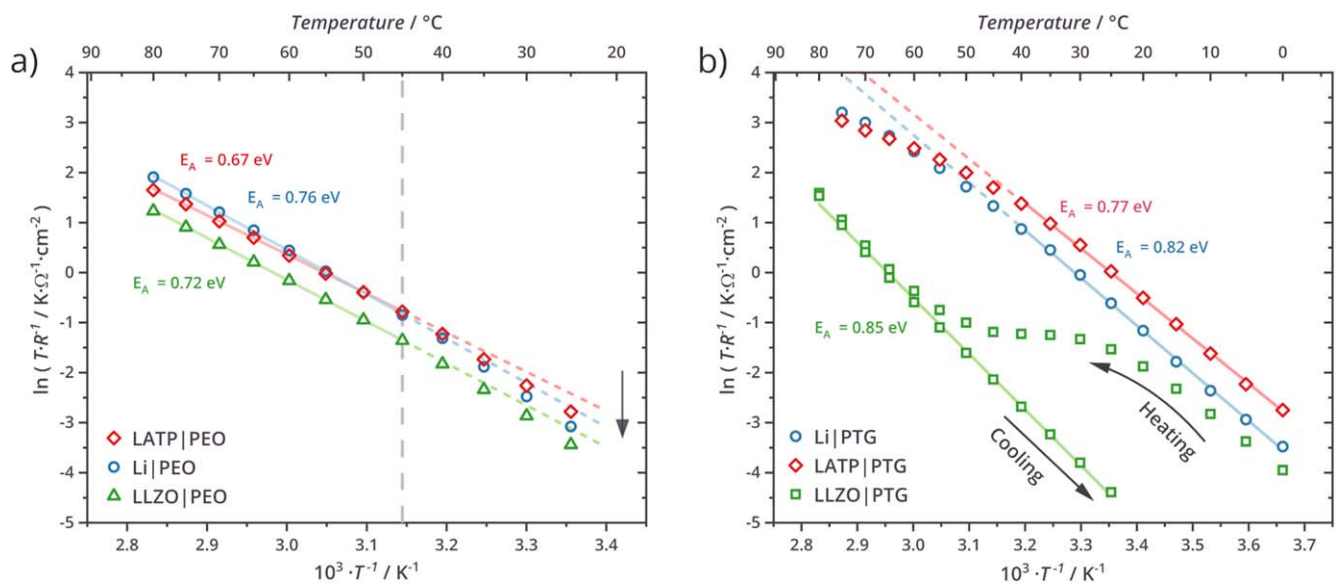


**Figure 3.** Arrhenius plots of the area normalized resistance of the different interfaces for (a) the PEO-based electrolyte during cooling and (b) the PTG-based electrolyte. Lines represent the obtained fits for the activation energy values. The deviations from linearity are discussed in the main text.

values at 60 °C are  $R_p = 30 \Omega\cdot\text{cm}^2$ ,  $28 \Omega\cdot\text{cm}^2$  and  $450 \Omega\cdot\text{cm}^2$  for PTG in contact with lithium metal, LATP and LLZO. These lower values can be directly attributed to the faster  $\text{Li}^+$  dynamics in the polymer phase and will be discussed in the next section.

For the PTG-based electrolyte, all interfaces also show relatively similar values for the activation energy:  $E_a = 0.77 \text{ eV}$ ,  $0.82 \text{ eV}$ ,  $0.85 \text{ eV}$  for the LATP|PTG, Li|PTG and LLZO|PTG interfaces, respectively. Compared to the values determined for PEO, a consistent slight increase was observed. We believe this discrepancy

to be linked to a stronger coordination of the  $\text{Li}^+$  by the side-chains present in PTG. At the same time, reorganization of the short side chains in PTG is likely faster compared to segmental motion in the long chains in PEO, leading to a higher number of available sites for the charge transfer at the interface with the ISE.<sup>33</sup>

The temperature dependence of the interface was studied, and the values obtained for the fitted EIS spectra are shown in Fig. 3b. Interestingly, a strong hysteresis in the determined PTG|LLZO interface resistance is observed between the heating and cooling

curves. This suggests that an irreversible process takes place between the two electrolytes at  $\sim 25^\circ\text{C}$ . The surface of LLZO is prone to contaminations, especially because of the strong basicity of the material. Exchange between  $\text{Li}^+$  in the ISE with  $\text{H}^+$  provided by PTG's terminating group likely leads to the formation of a low-conductivity layer on the LLZO surface.

This decomposition reaction was not strongly observed for PEO, likely because the PEO|ISE cells had to be maintained at  $60^\circ\text{C}$  for 24 h for lithiation of the reference electrode. During this time, side reactions between PE and LLZO may have taken place. Also, the higher MW of PEO compared to PTG translated to a higher concentration of OH terminal groups in the latter, i.e., protic functional group likely attacked by the ISE. Indeed, ATR-FTIR data support this interpretation, with a sharp band centered at  $3678\text{ cm}^{-1}$  in the spectra of the LLZO surface after contact with both PEs (Fig. 4a). The signal can be attributed to the phonons of newly formed LiOH, as such vibration is not present in LiTFSI or the PTG and PEO electrolytes (Fig. 4b).<sup>34</sup> On the other hand, no change in the spectra of the LATP pellets after contact with polymer was observed, suggesting that if an interphase is formed it is not detectable with this technique (Fig. 4c).

At temperatures above  $50^\circ\text{C}$ , the interfacial resistance determined for the Li|PTG and LATP|PTG deviates towards higher values compared to the linear trend traced from the lower temperature data (Fig. 3b). We propose that this deviation of the activation energy is caused by a transition in the transport dynamics, with the charge-transfer between the electrolytes being limiting below  $\sim 50^\circ\text{C}$ , while the  $\text{Li}^+$  transport from the bulk of the polymer to the interface being limiting above that temperature. To verify this phenomenon, the total cell impedance can be normalized to the high frequency “bulk” contribution of the electrolytes, which is dominated by the low conductivity of the polymer (Fig. 5). The change in resistances at different temperatures is connected to the activation energy of the investigated processes. Thus, if two processes have the same activation energy, the normalized EIS data at different temperature should overlap. This seems to be the case for these interfaces at temperatures higher than  $50^\circ\text{C}$ , as shown in Fig. 4a, where the change in total cell impedance is directly proportional to that of the high frequency contribution of the “bulk.” As this resistance is dominated by PTG-LiTFSI, this indicates that transport across the interface is only limited by the mobility of the ions in the PE close to the surface. As this transition is reversible when the cell is cooled down (Fig. 5b), other irreversible effects such as a change in surface area or chemical reactions can be excluded.

**Comparison of PEO and PTG interfaces with the ISEs and lithium.**—The results of the fits with equivalent circuits in Figs. 2 and 3 are summarized in Table 1 for each PE|ISE interface. Intriguingly, while the resistance of the interface between the PTG-based electrolyte and the ISEs is lower than for PEO, the activation energy for the charge transfer process is higher. Assuming simple CT kinetics, the interface resistance should be inversely proportional to the exchange current density of the activated charge-transfer process, which itself depends on the  $\text{Li}^+$  concentration ( $c_{\text{Li}^+}$ ) in the two electrolytes.<sup>35</sup> However, the  $c_{\text{Li}^+}$  in PTG was lower than  $c_{\text{Li}^+}$  in PEO, suggesting another mechanism to be relevant. A possible explanation for this discrepancy could involve the faster segmental relaxation of the short side-chains in PTG compared to the long chains in PEO, thereby increasing the attempt frequency of the jumps and the kinetic rate constant.<sup>36,37</sup> At the same time, the shorter chains are likely capable of better coordinating lithium ions, thereby increasing the energy required to remove the ion from its solvation sphere. Overall, CT resistance at the PE|LATP interface is lower than at the PE|LLZO interface, which is likely caused by unwanted reaction with LLZO.

**Conductivity of PTG-LATP composite electrolytes.**—Composite electrolytes are of particular interest as they could effectively resolve

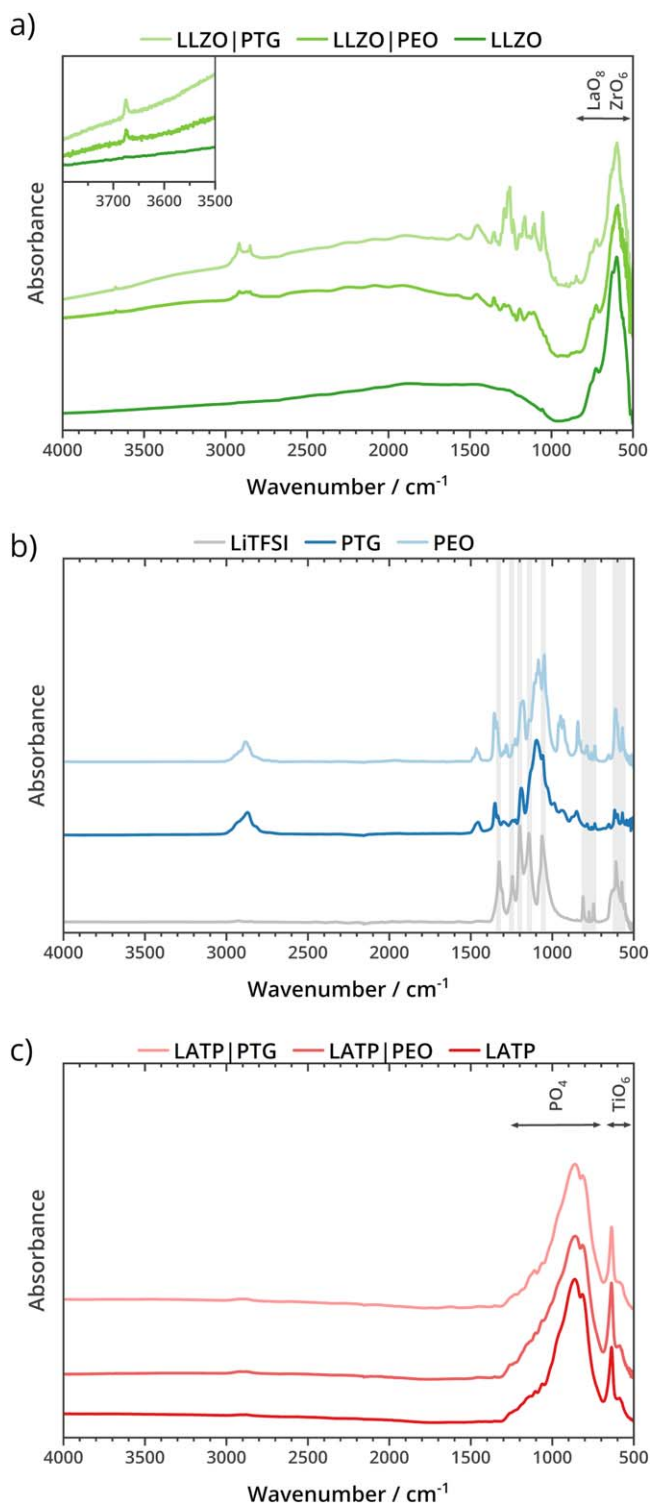


**Figure 4.** Stacked ATR-FTIR spectra of (a) polished surface of a LLZO pellet before and after being in contact with the PEs. The top left panel shows a magnification of the region between  $3800\text{ cm}^{-1}$  and  $3500\text{ cm}^{-1}$  with the characteristic LiOH band at  $3678\text{ cm}^{-1}$ . (b) Stacked spectra of the polymer electrolytes and LiTFSI. (c) Stacked spectra of the LATP pellets before and after being in contact with the PEs.

the processing issues shared by all ISEs while increasing the generally low ionic conductivity of PEs. However, the lithium-ion conductivity in CEs strongly depends on the volume fractions of the ISE and the polymer. In ISE-rich composites, a percolation network of inorganic particles can be formed acting as the main transport

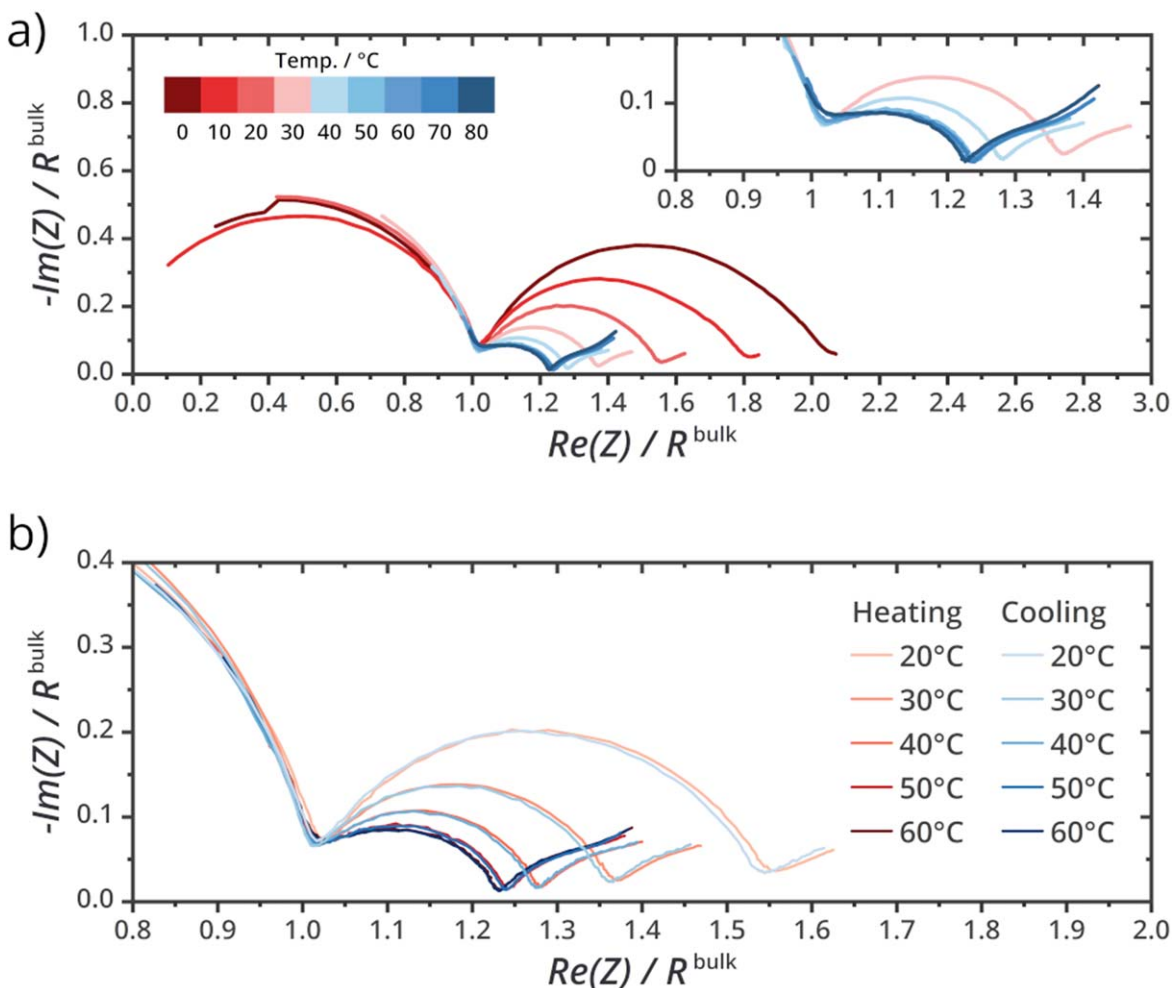


**Figure 5.** Nyquist plots of the EIS data at different temperature recorded between the two reference electrodes, corresponding to a PTG|LATP|PTG cell configuration. The data were normalized to the electrolyte bulk impedance  $R_{\text{bulk}}$ , dominated by the PE contribution. (a) At temperatures above 50 °C the total impedance becomes directly proportional to  $R_{\text{bulk}}$ , indicating that the limiting process is transport in the PE. (b) No change is observed upon heating/cooling, confirming reversibility of the transition.

**Table 1.** Characteristic values of the interface resistance, capacitance and activation energy for the ISEs and PEs investigated in this work. The value  $\alpha$  is the coefficient of the constant phase element obtained from the fit.

	Temp. °C	LLZO PE			LATP PE			Li PE		
		$C_{\text{int}}$ $\mu\text{F}\cdot\text{cm}^{-2}$	$R_{\text{int}}$ $\Omega\cdot\text{cm}^2$	$\alpha$	$C_{\text{int}}$ $\mu\text{F}\cdot\text{cm}^{-2}$	$R_{\text{int}}$ $\Omega\cdot\text{cm}^2$	$\alpha$	$C_{\text{int}}$ $\mu\text{F}\cdot\text{cm}^{-2}$	$R_{\text{int}}$ $\Omega\cdot\text{cm}^2$	$\alpha$
PEO	25	0.41	9300	0.83	2.6	3000	0.88	1.2	3200	0.79
	60	0.43	460	0.84	2.7	146	0.91	1.3	110	0.81
			$E_{\text{A}} = 0.72$ eV			$E_{\text{A}} = 0.67$ eV			$E_{\text{A}} = 0.76$ eV	
PTG	25	0.77	1280	0.80	2.9	265	0.83	3.0	550	0.82
	60	0.44	470	0.77	2.0	28	0.77	1.8	30	0.79
			$E_{\text{A}} = 0.85$ eV			$E_{\text{A}} = 0.77$ eV			$E_{\text{A}} = 0.82$ eV	

mechanism for lithium ions. However, point contacts between particles limit the actual flux of ions attainable in this scenario. A possible strategy to overcome this problem is to mix low fractions of PE with the ISE having the polymer acting as a  $\text{Li}^+$  transport buffer layer between inorganic particles, i.e., effectively removing point contact issues. We explored this concept by studying the conductivity of ISE-rich composite electrolytes based on LATP and PTG, the material combination characterized by the lowest interface resistance in this study.

Conductivity data obtained from EIS spectra of LATP-PTG composite electrolytes with different fractions of polymer are

presented in Fig. 6. Gravimetric density and relative density for each composition are reported in Fig. S9. SEM images of LATP powders and the composite with 11.3 wt% of polymer electrolyte showing its uniform distribution around the ISE are shown in Fig. S10. The maximum partial conductivity attributable to the polymer was assumed to be proportional to the PTG volume fraction. This assumption neglects the influence of tortuosity and porosity; however, both these factors would decrease the effective conductivity. Hence, a measured conductivity in excess of these values could be attributed to a positive contribution by LATP in the composite. It is important to notice that such a contribution could be due to transport



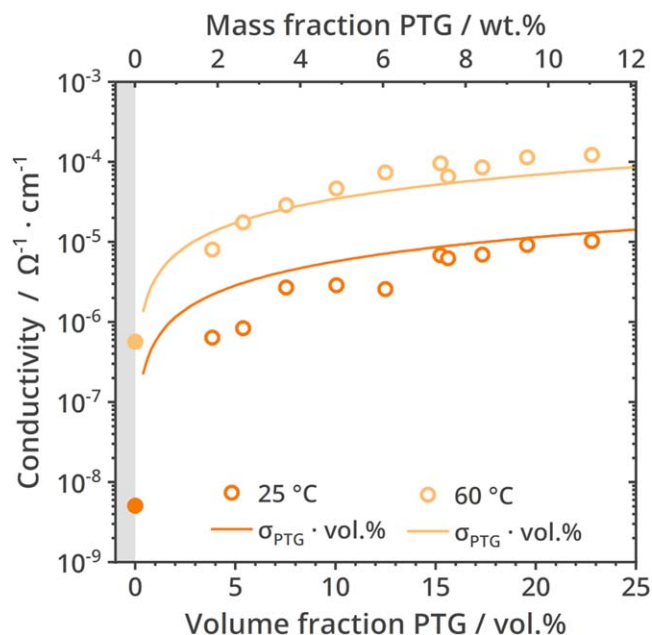


**Figure 6.** Conductivity as a function of the composition for mixtures of LATP powder and PTG-40 polymer electrolyte. Lines represent the maximum achievable conductivity if transport takes place only in the polymeric matrix, excluding tortuosity and porosity effects, calculated as the volume fraction of PTG multiplied by its conductivity at the given temperature. The conductivity excess at 60 °C can be attributed to transport along or across the boundary between the PE and ISE phases. Filled points correspond to cold-pressed powder of LATP.

both along and/or across the LATP|PTG interface. However, as PTG does not crystallize, we do not expect the transport along the interface to be significantly faster than the transport in the bulk polymer, as with PEO-based composites.

The conductivity of the composite electrolytes at 20 °C is always below the maximum expected conductivity of the polymer fraction. With increasing volume fraction of PTG, the discrepancy decreases, hinting at a lower penalty in effective conductivity due to tortuosity/porosity effects. This interpretation is supported by the increasing density of the composite and consequent decrease in porosity (Fig. S9). Overall, no positive contribution from LATP was observed at this temperature, suggesting that an interface resistance of 550  $\Omega\text{-cm}^2$  is too high to allow significant transport across both phases. A similar picture was found for the conductivity of the composite electrolytes at 60 °C. At low fractions of polymer, composites have lower conductivity than expected. A small “conductivity excess” was determined for compositions above 8 vol% of PTG. However, the increase is only modest compared to what would be attributable to the polymer phase alone.

The conductivity for the best performing composite with 9 wt% ( $\sim 20$  vol%) of PE is  $1 \cdot 10^{-4} \text{ S}\cdot\text{cm}^{-1}$  at 60 °C. The higher conductivity at this composition likely reflects the uncertainty in determining the electrolyte thickness ( $\sim 5\%$ ) rather than a real maximum in conductivity. At the same temperature, the conductivities of LATP and PTG are  $4 \cdot 10^{-3} \text{ S}\cdot\text{cm}^{-1}$  and  $4 \cdot 10^{-4} \text{ S}\cdot\text{cm}^{-1}$ , respectively. While some of the ionic transport in the composite electrolyte can be attributed to the presence of LATP, its contribution is not enough to match the characteristics of the single electrolytes. The relatively small interface resistance ( $28 \Omega\text{-cm}^2$  at 60 °C) between the two materials does not translate to improved properties of the composite. Plausibly, the numerous  $\text{Li}^+$  transfer steps between the two phases, necessary for long range transport in a particles-based composite, are detrimental for the overall conductivity, as no “fast-track” is available for the ions. By employing fibrous or micro-structured ISEs, the required number of charge transfer across phases may be reduced, while maximizing  $\text{Li}^+$  transport in the

inorganic phase with higher conductivity. Examples of such composite electrolytes with improved conductivity over particle based composites were reported recently.<sup>38–40</sup>

## Conclusions

In this work, the electrochemical properties of the interfaces between PEO- and PTG-based polymer electrolytes, and LATP and LLZO inorganic solid electrolytes, respectively, are characterized. PEO crystallization taking place below its melting point leads to an increase of the charge transfer resistance at the interface, while the non-crystallizing PTG did not show such deviations. After being in contact with the PEs, LiOH was observed on the surface of LLZO through ATR-FTIR, suggesting its decomposition and the formation of a more resistive interphase.

Given the relatively low value of  $28 \Omega\text{-cm}^2$  at 60 °C for the LATP|PTG charge-transfer resistance, the conductivity of ISE-rich composite electrolytes was investigated. At 60 °C, a modest excess of conductivity compared to the maximum expected value at low volume fractions was measured. However, the total conductivity of the CEs was still lower than that of the single PTG and LATP. To achieve particle-based CEs with higher conductivity, lower interface resistances between ISE|PE need to be achieved.

## Acknowledgments

The authors are grateful to Dr. Thorben Krauskopf for the preparation of the LLZO pellets. E. T., F. H. R. and J. J. thank the German Federal Ministry of Education and Research (BMBF) for funding of the projects EvaBatt (03XP0134C) and AdamBatt (03XP0305C).

## ORCID

Felix H. Richter <https://orcid.org/0000-0002-6587-7757>

Jürgen Janek <https://orcid.org/0000-0002-9221-4756>

## References

- J. Janek and W. G. Zeier, “A solid future for battery development.” *Nat. Energy*, **1**, 16141 (2016).
- Y. Zhu, X. He, and Y. Mo, “First principles study on electrochemical and chemical stability of solid electrolyte–electrode interfaces in all-solid-state Li-ion batteries.” *J. Mater. Chem. A*, **4**, 3253 (2016).
- Y. Xiao, Y. Wang, S.-H. Bo, J. C. Kim, L. J. Miara, and G. Ceder, “Understanding interface stability in solid-state batteries.” *Nat Rev Mater*, **5**, 105 (2020).
- J. G. Connell, T. Fuchs, H. Hartmann, T. Krauskopf, Y. Zhu, J. Sann, R. Garcia-Mendez, J. Sakamoto, S. Tepavcevic, and J. Janek, “Kinetic vs thermodynamic stability of LLZO in contact with lithium metal.” *Chem. Mater.*, **32**, 10207 (2020).
- L. Miara, A. Windmüller, C.-L. Tsai, W. D. Richards, Q. Ma, S. Uhlenbruck, O. Guillon, and G. Ceder, “About the compatibility between high voltage spinel cathode materials and solid oxide electrolytes as a function of temperature.” *ACS Appl. Mater. Interfaces*, **8**, 26842 (2016).
- M. Keller, A. Varzi, and S. Passerini, “Hybrid electrolytes for lithium metal batteries.” *J. Power Sources*, **392**, 206 (2018).
- X. Yu and A. Manthiram, “A review of composite polymer-ceramic electrolytes for lithium batteries.” *Energy Storage Mater.*, **34**, 282 (2021).
- S. Sen, E. Trevisanello, E. Niemöller, B.-X. Shi, F. J. Simon, and F. H. Richter, “The role of polymers in lithium solid-state batteries with inorganic solid electrolytes.” *J. Mater. Chem. A*, **9**, 18701 (2021).
- F. J. Simon, M. Hanauer, A. Henss, F. H. Richter, and J. Janek, “Properties of the interphase formed between argyrodite-type Li6PS5Cl and polymer-based PEO10:LiTFSI.” *ACS Appl. Mater. Interfaces*, **11**, 42186 (2019).
- F. J. Simon, M. Hanauer, F. H. Richter, and J. Janek, “Interphase formation of PEO20:LiTFSI-Li6PS5Cl composite electrolytes with lithium metal.” *ACS Appl. Mater. Interfaces*, **20212**, 11713 Published Online: 2/25/2020.
- J. Zagórski, J. M. López del Amo, M. J. Cordill, F. Aguesse, L. Buannic, and A. Llordés, “Garnet–polymer composite electrolytes: new insights on local li-ion dynamics and electrodeposition stability with Li metal anodes.” *ACS Appl. Energy Mater.*, **2**, 1734 (2019).
- M. Weiss, F. J. Simon, M. R. Busche, T. Nakamura, D. Schröder, F. H. Richter, and J. Janek, “From liquid- to solid-state batteries: ion transfer kinetics of heteroionic interfaces.” *Electrochem. Energy Rev.*, **3**, 221 (2020).
- J. Liu et al., “The Interface between Li6.5La3Zr1.5Ta0.5O12 and Liquid Electrolyte.” *Joule*, **4**, 101 (2020).
- X. C. Chen, X. Liu, A. Samuthira Pandian, K. Lou, F. M. Delnick, and N. J. Dudney, “Determining and minimizing resistance for ion transport at the polymer/ceramic electrolyte interface.” *ACS Energy Lett.*, **4**, 1080 (2019).

15. S. Kalnaus, A. S. Sabau, W. E. Tenhaeff, N. J. Dudney, and C. Daniel, "Design of composite polymer electrolytes for Li ion batteries based on mechanical stability criteria." *J. Power Sources*, **201**, 280 (2012).
16. A. Gupta and J. Sakamoto, "Controlling Ionic Transport through the PEO-LiTFSI/LLZTO Interface." *Electrochim. Soc. Interface*, **28**, 63 (2019).
17. F. Langer, M. S. Palagonia, I. Bardenhagen, J. Glenneberg, F. La Mantia, and R. Kun, "Impedance spectroscopy analysis of the lithium ion transport through the Li<sub>7</sub>La<sub>3</sub>Zr<sub>2</sub>O<sub>12</sub>/PEO interface." *J. Electrochem. Soc.*, **164**, A2298 (2017).
18. D. Brogioli, F. Langer, R. Kun, and F. La Mantia, "Space-charge effects at the Li<sub>7</sub>La<sub>3</sub>Zr<sub>2</sub>O<sub>12</sub>/poly(ethylene oxide) interface." *ACS Appl. Mater. Interfaces*, **11**, 11999 (2019).
19. T. Zhang, N. Imanishi, S. Hasegawa, A. Hirano, J. Xie, Y. Takeda, O. Yamamoto, and N. Sammes, "Water-stable lithium anode with the three-layer construction for aqueous lithium-air secondary batteries." *Electrochim. Solid-State Lett.*, **12**, A132 (2009).
20. J. A. Isaac, L. R. Mangani, D. Devaux, and R. Bouchet, "Electrochemical impedance spectroscopy of PEO-LATP model multilayers: ionic charge transport and transfer." *ACS Appl. Mater. Interfaces*, **14**, 13158 (2022), Published Online: Mar. 8, 2022.
21. M. R. Busche, T. Leichtweiss, C. Fiedler, T. Drossel, M. Geiss, M. Weiß, A. Kronenberger, D. A. Weber, and J. Janek, "The formation of the solid-liquid electrolyte interphase (SLEI) on NASICON-type glass ceramics and LiPON." (2020).
22. M. R. Busche, T. Drossel, T. Leichtweiss, D. A. Weber, M. Falk, M. Schneider, M.-L. Reich, H. Sommer, P. Adelhelm, and J. Janek, "Dynamic formation of a solid-liquid electrolyte interphase and its consequences for hybrid-battery concepts." *Nat. Chem.*, **8**, 426 (2016), Published Online: 3/14/2016.
23. F. J. Simon, L. Blume, M. Hanauer, U. Sauter, and J. Janek, "Development of a wire reference electrode for lithium all-solid-state batteries with polymer electrolyte: FEM simulation and experiment." *J. Electrochem. Soc.*, **165**, A1363 (2018).
24. M. Andrei, J. Cowie, and P. Prosperi, "Polymer electrolytes based on polyphosphazene with pendant 12-crown-4 groups and monovalent salts." *Electrochim. Acta*, **37**, 1545 (1992).
25. S. Pantaloni, S. Passerini, F. Croce, B. Scrosati, A. Roggero, and M. Andrei, "Electrochemical characterization of a class of low temperature conducting polymer electrolytes." *Electrochim. Acta*, **34**, 635 (1989).
26. Q. Ma, Q. Xu, C.-L. Tsai, F. Tietz, and O. Guillon, "A novel sol-gel method for large-scale production of nanopowders: preparation of Li<sub>1.5</sub>Al<sub>0.5</sub>Ti<sub>1.5</sub>(PO<sub>4</sub>)<sub>3</sub> as an example." *J. Am. Ceram. Soc.*, **99**, 410 (2016).
27. B. Kim, C.-G. Chae, Y. Satoh, T. Isono, M.-K. Ahn, C.-M. Min, J.-H. Hong, C. F. Ramirez, T. Satoh, and J.-S. Lee, "Synthesis of hard-soft-hard triblock copolymers, poly(2-naphthyl glycidyl ether)- block -poly[2-(2-methoxyethoxy)ethoxy]ethyl glycidyl ether]- block -poly(2-naphthyl glycidyl ether), for solid electrolytes." *Macromolecules*, **51**, 2293 (2018).
28. W. Zhang et al., "Interfacial processes and influence of composite cathode microstructure controlling the performance of all-solid-state lithium batteries." *ACS Appl. Mater. Interfaces*, **9**, 17835 (2017), Published Online: May. 16, 2017.
29. M. Marzantowicz, J. R. Dygas, F. Krok, J. L. Nowiński, A. Tomaszewska, Z. Florjańczyk, and E. Zygadło-Monikowska, "Crystalline phases, morphology and conductivity of PEO:LiTFSI electrolytes in the eutectic region." *J. Power Sources*, **159**, 420 (2006).
30. L. Aguilera, S. Xiong, J. Scheers, and A. Matic, "A structural study of LiTFSI-tetraglyme mixtures: From diluted solutions to solvated ionic liquids." *J. Mol. Liq.*, **210**, 238 (2015).
31. J.-B. Jorcin, M. E. Orazem, N. Pébère, and B. Tribollet, "CPE analysis by local electrochemical impedance spectroscopy." *Electrochim. Acta*, **51**, 1473 (2006).
32. G. Dlubek, D. Kilburn, V. Bondarenko, J. Pionteck, R. Krause-Rehberg, and M. A. Alam., "Characterisation of free volume in amorphous materials by PALS in relation to relaxation phenomena." *24th Arbeitskreisstagung 'Nichtkristalline Strukturen' of DGGK*, 203 (2003).
33. M. A. Ratner, P. Johansson, and D. F. Shriver, "Polymer electrolytes: ionic transport mechanisms and relaxation coupling." *MRS Bull.*, **25**, 31 (2000).
34. L. H. Jones, "The infrared spectra and structure of LiOH, LiOH·2 O and the deuterium species. remark on fundamental frequency of OH-." *J. Chem. Phys.*, **22**, 217 (1954).
35. M. Schleutker, J. Bahner, C.-L. Tsai, D. Stolten, and C. Korte, "On the interfacial charge transfer between solid and liquid Li+ electrolytes." *Physical chemistry chemical physics: PCCP*, **19**, 26596 (2017).
36. M. E. Ries, P. G. Klein, M. G. Brereton, and I. M. Ward, "Proton NMR study of rouse dynamics and ideal glass transition temperature of poly(ethylene oxide) LiCF<sub>3</sub>SO<sub>3</sub> complexes." *Macromolecules*, **31**, 4950 (1998).
37. K. Se, K. Adachi, and T. Kotaka, "Dielectric relaxations in poly (ethylene oxide): dependence on molecular weight." *Polym. J.*, **13**, 1009 (1981).
38. W. Liu, S. W. Lee, D. Lin, F. Shi, S. Wang, A. D. Sendek, and Y. Cui, "Enhancing ionic conductivity in composite polymer electrolytes with well-aligned ceramic nanowires." *Nat. Energy*, **2**, 17035 (2017).
39. H. Zhai, P. Xu, M. Ning, Q. Cheng, J. Mandal, and Y. Yang, "A flexible solid composite electrolyte with vertically aligned and connected ion-conducting nanoparticles for lithium batteries." *Nano Lett.*, **17**, 3182 (2017), Published Online: 4/24/2017.
40. M. Zhang, P. Pan, Z. Cheng, J. Mao, L. Jiang, C. Ni, S. Park, K. Deng, Y. Hu, and K. K. Fu, "Flexible, mechanically robust, solid-state electrolyte membrane with conducting oxide-enhanced 3D nanofiber networks for lithium batteries." *Nano Lett.*, **21**, 7070 (2021), Published Online: Jun. 8, 2021.